Review of Scientific Instruments

Apparatus and method for the growth of epitaxial complex oxides on native amorphous SiO_2 surface of (001) oriented single crystal silicon

Cite as: Rev. Sci. Instrum. **89**, 085102 (2018); https://doi.org/10.1063/1.5040390
Submitted: 17 May 2018 . Accepted: 09 July 2018 . Published Online: 03 August 2018

Prahallad Padhan, Umesh Kumar Sinha, and Antarjami Sahoo

View Online

Export Citation

CrossMark

ARTICLES YOU MAY BE INTERESTED IN

A versatile ion beam spectrometer for studies of ion interaction with 2D materials
Review of Scientific Instruments **89**, 085101 (2018); https://doi.org/10.1063/1.5037798

Strain-dependent magnetic phase diagram of epitaxial $La_{0.67}Sr_{0.33}MnO_3$ thin films
Applied Physics Letters **76**, 2421 (2000); https://doi.org/10.1063/1.126363

Design and laboratory testing of a MEMS accelerometer array for subsidence monitoring
Review of Scientific Instruments **89**, 085103 (2018); https://doi.org/10.1063/1.5036666

Lock-in Amplifiers
up to 600 MHz

© 2018 Author(s).

REVIEW OF SCIENTIFIC INSTRUMENTS **89**, 085102 (2018)

Apparatus and method for the growth of epitaxial complex oxides on native amorphous SiO_2 surface of (001) oriented single crystal silicon

Prahallad Padhan, Umesh Kumar Sinha, and Antarjami Sahoo
Department of Physics, Indian Institute of Technology Madras, Chennai 600036, India

(Received 17 May 2018; accepted 9 July 2018; published online 3 August 2018)

The design, fabrication, and performance of an apparatus for the deposition of complex oxides with highly uniform thicknesses at controllable deposition rates over large area, even on the native amorphous SiO_2 layer of (001) oriented single crystal Si, are described. The apparatus makes use of the lateral port of a spherical chamber. The port is maintained at uniform temperature, and it houses a substrate heater. The deposition process is controlled by varying different parameters such as target-to-substrate distance, sputtering power, sputtering gas atmosphere, substrate temperature, and pulsed plasma growth. The system has been tested by growing a series of $La_{0.7}Sr_{0.3}MnO_3$ thin films on Si. The systematic strain relaxation and thus the tunable magnetic properties along with the presence of high-quality surface morphology of the films indicate that the designed system could be used to fabricate different components of oxide electronics-based devices over larger area. *Published by AIP Publishing.* https://doi.org/10.1063/1.5040390

I. INTRODUCTION

The structural distortion has been induced to change the charge, spin, and orbital states in the bulk complex oxides by chemical doping, pressure, and temperatures.[1,2] In addition, the structure of the complex oxides has also been modified by the preparation of the material in the form of thin film which stimulates novel functionalities in electronic transport and magnetic and optical properties.[3–5] In particular, the possibility of externally modifying the properties of thin-film complex oxides by epitaxial strain or artificial boundaries and thus potentially generating novel properties at the interfaces open a new perspective. Nevertheless, the thin-film microelectronics and optoelectronics industries have manifested the explosive growth in communications and in information processing, storage, and display applications.[6] The excellent performance of the thin-film devices requires high-quality thin films that are free from pinholes and cracks, have densely packed grains, and have strong adherence with the substrate. The general requirement for the synthesis of epitaxial thin film of multi-component oxide is the stringent control of the composition during the deposition process. Numerous thin-film growth techniques have been investigated for the epitaxial growth of the oxide films. The film growth techniques that have been successfully employed in the synthesis of epitaxial oxide materials include physical vapour deposition techniques, such as co-evaporation, molecular beam epitaxy (MBE), pulsed-laser deposition (PLD), and sputtering, as well as chemical vapour deposition technique.[7] With physical vapour deposition of oxides, the phase constituents are delivered as a flux of individual atoms, ions, or simple oxide species. Atomic-level control of the film growth process is possible with the most *in situ* growth approaches, thus enabling the formation of novel multilayer structures. However, a critical issue in the fabrication of such devices is the growth of high-quality thin films over a large area with uniform thicknesses,[8] efficient control of properties, and stoichiometric compositions. In addition, the undesirable deposition of particulates during the preparation of thin films influences the physical properties, which is frequently found in the thin films grown using PLD technique.[8]

The sputtered deposition is a versatile technique to fabricate high-quality thin films of a broad range of materials. Several sputtered deposition techniques have been used in the growth of oxide films, including on-axis dc magnetron sputtering, cylindrical magnetron sputtering, ion-beam sputtering, and off-axis sputtering. In on-axis geometry, the substrate and target face each other.[7,9–12] This is the optimal geometry for maximum deposition rate but can result in film damage due to the bombardment of the energetic species from the plasma on the film surface. An alternative to this is an off-axis geometry where the film growth rate is significantly reduced, which is undesirable for the commercialization of oxide-based electronic devices.[9] Better uniformity has been obtained by Xi *et al.*[10] by using inverted cylindrical magnetron sputtering. However, the fabrication of complex oxide cylindrical target is very expensive. Li *et al.*[11] have sputtered at very high pressure (600 mTorr) in order to decrease the kinetic energy of the particles, and consequently, backscattering is reduced. The uniformity of the resulting film is usually poor since the substrate has to be placed at the center of the sputtering target and away from the erosion area.

In this article, we describe the development of an apparatus and the method for sputtered deposition of transition metal oxide thin film on single crystal substrate with native amorphous oxide layer.

II. CHAMBER DESIGN AND FABRICATION

The physical vapour deposition technique primarily consists of four different apparatuses such as chamber with the magnetron, heater assembly, RF power supply, and pumping system. The system was designed in such a way that it (i) generates a horizontally orientated plasma, (ii) offers larger

cathode surface in front of the plasma, (iii) places the substrate heater inside the specified port, (iv) maintains a uniform temperature of that port wall using the cooled water, and (v) provides an option to customise the target-to-substrate distance. A stainless steel sphere with 350 mm diameter forms the basis of the chamber, which offers the smallest surface-to-volume ratio than any other shapes. The perspective cross-sectional view of the chamber is shown in Fig. 1. The ports (1) and (2) house the substrates mounted to the heater. These ports are designed to be maintained at uniform temperature by flowing cooled water. The chamber is filled with the reactive sputtering gas by flowing it through port (3). The non-reactive gases such as oxygen or nitrogen are passed into the chamber through port (4). The pressure inside the chamber is controlled with great accuracy by using a gate valve attached to the bottom port (5). The gate valve is mounted on the turbo-pump having maximum of 49 000 rotations/min. This high vacuum pump backed by the rotary pump can reduce the chamber pressure to the order of 10^{-6} mbar. The pressure inside the chamber is monitored by using a Pirani gauge connected to port (6) and a penning gauge mounted on a port, which is not shown in the sketch in Fig. 1. The top port (7) is sealed by a flange that holds an assembly of four magnetrons [only two, (8) and (9), are shown] at the center of the chamber, wherein the target assembly attached to the magnetrons can be rotated using mechanical assembly (10) to align the target (11) coaxially with the substrate (12) placed on the heater (13). The target and the substrate face each other and the target can be moved symmetrically around the central axis of this on-axis sputtering technique. The present technique requires a single target to grow complex oxides compared with the multiple targets used in the case of co-sputtered techniques.[13] Therefore, this technique provides an advantage to grow technologically important heterostructures of four different materials.

The magnetron assembly is positioned at the center of the chamber by moving the shaft (14) using the mechanical assembly (10) attached to the flange. The surfaces of magnetrons mounted to the shaft are parallel to the vertical axis of the chamber. The magnetron assembly is designed to rotate around its axis to place the target in front of the substrate and the cold water can be flown through it for the removal of excessive heat produced by the magnetron and target, fixed on its surface. The target is typically mounted on the magnetron's flat surface in such a way that it is electrically isolated from the chamber. The target is connected to an N-type male (15) which is connected to a voltage source to maintain a negative voltage with respect to the electrically grounded chamber. A DC power supply or an RF power supply controlled by an impedance matching network is connected to the magnetron. The electrons generated by the applied negative biased voltage eject the ions and/or atoms from the target after bombardment. The system is suitable to achieve the required negative biased voltage for different types of materials such as metallic, simple, and complex ceramic targets.

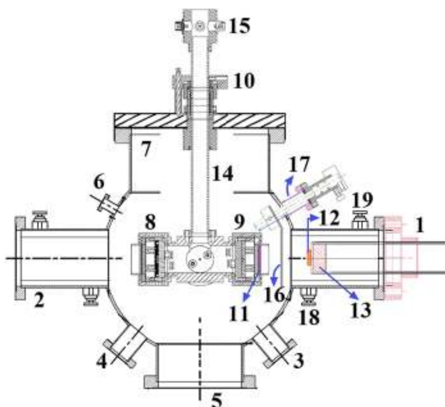

FIG. 1. Schematic of the cross section of the sputtered deposition chamber: (1) and (2) ports house heaters, (3) reactive gas inlet, (4) non-reactive gas inlet, (5) port connects to the gate valve to separate the pumping system, (6) port links to Pirani gauge head, (7) port houses magnetron assembly, (8) and (9) magnetrons, (10) mechanical rotation assembly, (11) target, (12) substrate, (13) heater, (14) shaft, (15) N-type male connector, (16) shutter, (17) port houses shutter rotation assembly, (18) cold water inlet, and (19) water outlet.

After achieving the base pressure $\sim 10^{-6}$ mbar inside the chamber, it is filled with appropriate pressure of the argon and oxygen gases and then a suitable negative voltage is applied to the sputtering target to generate the plasma. The flux of energetic electrons generated in the sputter gas is directed toward the target by the application of magnetic field, which is responsible for the ejection of materials from the target to form the plasma. The atoms and ions present in the plasma deposit on the surface of the substrate mounted on the heater (13). The heater is designed for maintaining a constant substrate temperature upto 750 °C during the deposition. High deposition rate of complex oxides usually provides the growth of parasitic impurity phases, non-stoichiometry, and very different physical properties compared with its bulk. The present deposition apparatus provides controllable parameters such as (i) variation in target-to-substrate distance, (ii) precise control of chamber pressure during the deposition, and (iii) pulsed plasma deposition (PPD). The heater is configured to move along its axis to place the deposition surface of the substrate at different locations of the plasma; i.e., the distance between the target and the substrate can be varied from 8 cm to 20 cm. In order to provide the desired thickness and structural uniformity as well as slow and controlled growth rate, PPD is performed with various combinations of deposition time and waiting time by opening and closing the shutter (16), respectively, in front of the port (1) inside the chamber. The shutter is configured to rotate through port (17) for switching on and off the deposition on the substrate, which generates the pulsed plasma for different hold durations and provides relaxation during the growth. This geometry, in combination with pulsed deposition, facilitates the deposition of a thin film having the stoichiometry of the target and uniformity in the thickness over the entire deposition surface. We have been able to achieve a minimum growth rate of ~1.8 nm/min using the designed technique, which favours the layer-by-layer stacking of complex oxide epitaxial thin films.

III. SYSTEM PERFORMANCE

A. Fabrication of target

A highly dense target is prepared through the standard solid-state reaction method. The $La_{0.7}Sr_{0.3}MnO_3$ (LSMO)

target is made from the dried chemicals such as 99.9% pure La_2O_3, $SrCO_3$, and Mn_2O_3, which act as the starting materials. These dried chemicals were taken in stoichiometric proportion and grinded thoroughly using mortar and pestle for at least 2 h to obtain a homogeneous mixture. After grinding for 2 h, the mixture was calcinated at 850–1100 °C for 12–24 h. The calcination process removes the carbon content from the mixture by dissociating the carbonates into CO_2 and O. In addition, this step also helps in removing the water content and volatile impurities. The grinding and calcination processes were repeated for three times to ensure the homogenization as well as the carbon-free oxide mixture. The powder was then pelletized at high pressure (~30 KPa) in the form of a disc with 2 in. diameter. And finally, the pellet is sintered at high temperatures (1200–1300 °C) for 12 h to get the highly dense LSMO target.[14]

B. Fabrication of thin films

The highly dense ceramic target of LSMO was mounted on the magnetron. Then, a piece of (001) oriented single crystal Si substrate was cleaned successively by acetone and methanol in an ultrasonic bath. The dried substrate was glued on the heater using silver paste. After drying the silver paste, the heater was inserted into the port and the substrate was placed at 120 mm away from the target surface. The chamber was evacuated to 5.6×10^{-6} mbar pressure and the cooled water was circulated through the required locations. Then, the temperature of the substrate heater was set to 700 °C. Once the required temperature is reached, the Ar and O_2 gas flow was set to 6.1 SCCM and 18.2 SCCM, respectively. The gate valve was throttled to achieve a chamber pressure of $\sim 10^{-2}$ mbar. Then, the RF power was slowly increased to generate the plasma. The depositions were performed in pulsed mode at 7×10^{-3} mbar pressure by keeping the sputtering power density at 2.96 W/cm^2. Thin films were grown for different durations by altering the opening and closing of the shutter for a period of 30 s and 30 s, respectively.

C. Result and discussion

The thin films were comprehensively investigated using a variety of characterization techniques. The crystal structures of the thin films were verified from the X-ray diffraction (XRD) spectra and the film thicknesses were determined from the low-angle X-ray reflectivity patterns. Atomic Force Microscopy (AFM) was employed to analyze the surface morphology and roughness. The magnetic properties have been investigated using a superconductive quantum interference device (SQUID) magnetometer.

The typical room temperature θ−2θ XRD patterns of thin films of LSMO grown on (001) oriented single crystal Si substrates are shown in Fig. 2. The angular position of the (002) Braag's peak of the Si offers its lattice parameter $a_{\mathrm{Si}} = 5.432$ Å,[15] which is very large for the epitaxial growth of LSMO ($a_{\mathrm{LSMO}} = 3.88$ Å).[16] However, the $d_{110} = 3.841$ Å of Si offers an epitaxial growth of LSMO with a lattice mismatch of $\frac{a_{Si}-a_{LSMO}}{a_{Si}} = -1.01\%$. The XRD patterns reveal only the noticeable (00l) oriented peaks of LSMO and the substrates without any evidence of additional peaks, indicating the epitaxial and highly oriented growth of perovskite structure of LSMO on Si substrates. The out-of-plane lattice parameter $c \approx 3.91$ Å obtained from the (001) diffraction peak of 95 Å thick LSMO film indicates that the LSMO experiences tensile strain $\frac{a_{\mathrm{LSMO}-BULK}-a_{\mathrm{LSMO}-FILM}}{a_{\mathrm{LSMO}-BULK}} = -0.77\%$ along the growth directions. As the LSMO thickness increases to 180 Å, the strain becomes −0.21%. The observed systematic strain relaxation of LSMO film on Si indicates that the influence of native SiO_2 on the epitaxial growth is not significant. By contrast, it is reported that the chemisorption during the deposition of binary, ternary, and multi-component oxides leads to the formation of an interfacial SiO_2, which is responsible for the lack of epitaxy and the degradation of film quality. Hence, a template layer is usually grown on Si before the growth of functional oxides.[17–19] Even with the template $SrTiO_3$ (STO), the $La_{0.67}Ba_{0.33}MnO_3$ grown on Si substrate using PLD is polycrystalline rather than highly oriented.[19] The SiO_2, which is used as a gate dielectric in metal-oxide-semiconductor field-effect transistor in microelectronics industry, increases the static power consumption due to the quantum mechanical tunneling. Therefore, the direct integration of different oxides with high K can be seen as an alternative to SiO_2.[20] The epitaxial growth of oxides with high temperature superconductivity, ferroelectricity, colossal magnetoresistance, etc., on bare Si wafer is technologically important in terms of fabricating ferroelectric field effect transistor, microelectromechanical systems, and ferroelectric random access memory devices.[20] Thin films of LSMO grown on Si using PLD does not yield highly oriented crystal structure.[15] An unforeseen elongation of out-of-plane lattice parameter of LSMO grown on STO using PLD has been observed.[21] In contrast, the anticipated out-of-plane elongation of the lattice parameter of LSMO/Si grown using our designed sputtering system is realized (see Fig. 2). The systematic strain relaxation observed in XRD patterns of LSMO indicates its coherent growth on bare Si substrates using this RF sputtering technique.[22] The coherent growth of

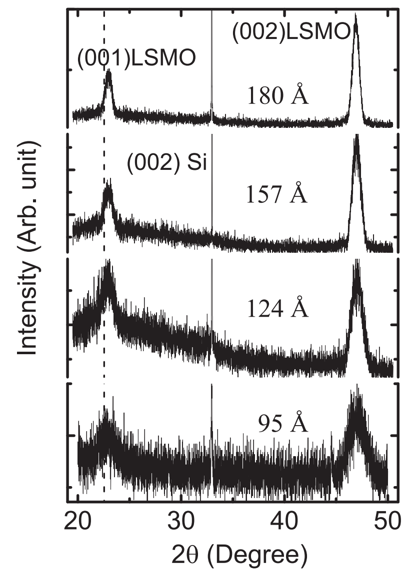

FIG. 2. $\theta-2\theta$ X-ray diffraction patterns of four $La_{0.7}Sr_{0.3}MnO_3$ thin films grown on (001) oriented Si substrates.

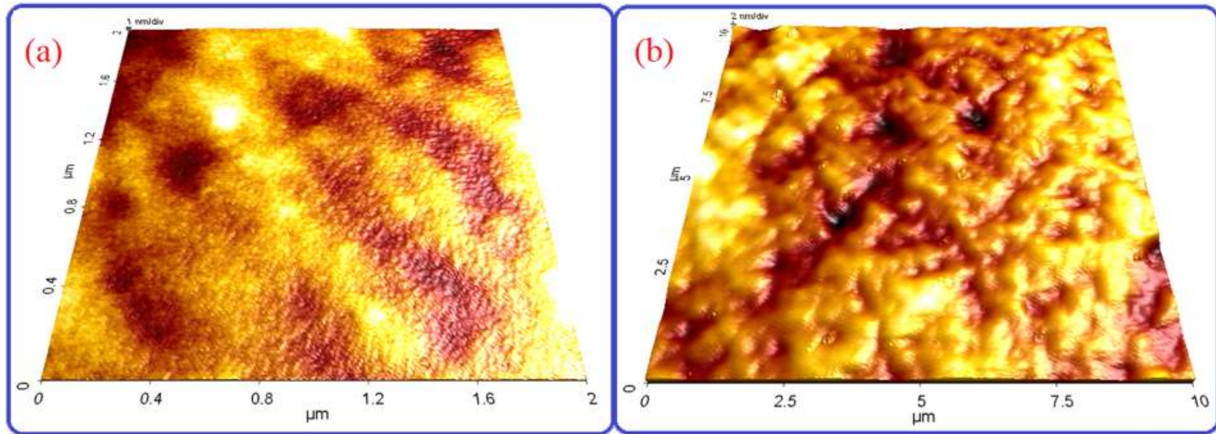

FIG. 3. Atomic Force Microscopic images of (a) 95 Å and (b) 180 Å thick $La_{0.7}Sr_{0.3}MnO_3$ films grown on (001) oriented Si substrates.

the LSMO on bare Si can be used as the microelectronics components.

Figure 3 shows the AFM images of the surface morphologies of the 95 and 180 Å thick LSMO grown on the Si substrates. It is very clear that the 95 Å thick LSMO is atomically smooth [see Fig. 3(a)] with 5.69 Å root mean square (RMS) roughness, which is less than 2 unit cell (u.c.). This also indicates the layer-by-layer growth (step-flow growth) of LSMO on Si.[23] Similar type of smooth morphology is observed when LSMO is grown by PLD[24] and when grown at very high temperature followed by post-annealing at 1000 °C by RF sputtering technique[23] on STO. However, as the LSMO thickness is increased to 180 Å, the RMS roughness increases close to 2 u.c. (9.03 Å) and the domain size increases due to coalescence. The observed RMS roughness is significantly smaller than the 220 Å $La_{0.6}Sr_{0.4}MnO_3/SrTiO_3/Si$ grown using pulsed laser deposition.[25] In addition, the peak-to-valley height increases from 43 Å to 49 Å, suggesting a uniform growth of LSMO over the entire area.

The temperature-dependent field-cooled (FC) magnetization (M(T)) measurements of these LSMO thin films have been performed with the 0.01 T in-plane field. Figure 4 shows the FC M(T) of different LSMO thin films grown on Si. The M(T) of all thin films exhibit ferromagnetic to paramagnetic transition at Curie temperature (T_C). The T_C of 95 Å thick LSMO film is 271 K, which is lower than that of the bulk T_C = 369 K.[26] However, as the film thickness increases, the T_C also increases and becomes 330 K for 180 Å thick film. The variation in T_C with the LSMO film thickness is consistent with the variation in out-of-plane lattice parameter. Similar variation in T_C because of the substrate-induced strain or finite size effect has been reported for $La_{0.7}Sr_{0.3}MnO_3$ thin films grown on single crystal cubic oxide substrate STO using pulsed laser deposition.[22,27] The observed reduction in the T_C of LSMO thin film compared with that of the bulk is generally interpreted by considering a strain-induced distortion of MnO_6 octahedra based on Jahn-Teller distortion theory.[28] However, the T_C of LSMO thin films on Si is larger compared with that of the $La_{0.75}Sr_{0.25}MnO_3$ grown on $SrTiO_3$ and MgO substrates using RF or DC sputtering.[29] The observed T_C, close to the bulk LSMO, indicates the presence of perfect stoichiometry in the thin films of LSMO.[27]

The apparatus is facilitated to generate the plasma at low power and pressure. The plasma is oriented perpendicular to the plane of pumping, moves toward the substrate, which is confined inside a water-cooled port. The cooled surface of the inner wall forms an envelope of anode sheath to the plasma, which is a distinguished feature of this apparatus.[30] The anode sheath other than the substrate heater, shown in Fig. 5, is maintained at a constant temperature, which is lower than the room temperature, while the substrate temperature is maintained at

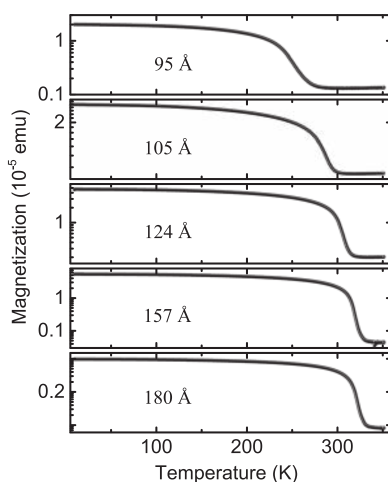

FIG. 4. Temperature-dependent 0.01 T field-cooled in-plane magnetization of five $La_{0.7}Sr_{0.3}MnO_3$ thin films grown on (001) oriented Si substrates.

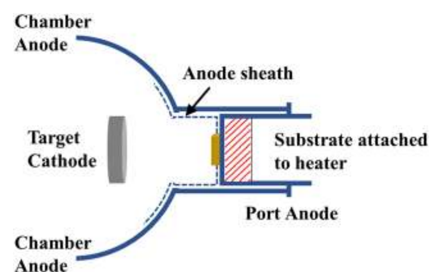

FIG. 5. Schematic of the cross section of the anode sheath envelope for the plasma inside the water-cooled port.

700 °C during the deposition. The energetic ions and/or neutral species are adsorbed by the inner wall of the chamber, maintained at low temperature, which reduces the undesired scattering of these species and offers the smooth growth of the film. This prevails the formation of plasma consisting of well-directed ionic and/or neutral species toward the substrate. In the plasma, the negative oxygen ions are accelerated by the cathode's electric field and bombarded on the film surface, the underlying substrate, and the inner wall of the water-cooled port. In the sputtering system shown in Fig. 1, the impact of negative oxygen ions can be tuned by (i) maintaining larger separation (8–20 cm) between the cathode and the anode, (ii) chamber pressure, and (iii) RF power. In addition, the apparatus provides an option for slow and relaxed film growth, which results in oriented nucleation for the epitaxial and stoichiometric crystal growth. The relaxation during the growth is achieved by closing and opening the shutter at different frequencies. Hence, it is quite apparent that the discussed sputtering apparatus is promoting the epitaxial growth of LSMO on the bare Si surface compared with that grown with or without buffer layer using MBE, PLD, and other sputtering techniques.

IV. CONCLUSION

In this article, a sputtering apparatus and a method for depositing thin film on a substrate, wherein the thin film is deposited inside the water-cooled port of sputtering chamber using pulsed plasma, have been presented. The ability to grow epitaxial thin film of complex transition metal oxide $La_{0.7}Sr_{0.3}MnO_3$ on single crystal Si substrate has been shown using the designed sputtering technique. The epitaxial LSMO shows smooth surface morphology with the epitaxial strain-induced anticipated magnetic properties. This discussed apparatus can be adapted for the deposition of thin films and heterostructures of other complex oxides such as piezoelectric, superconducting, multiferroic materials, etc., which have numerous potential applications.

ACKNOWLEDGMENTS

We greatly acknowledge the New Faculty Seed Grant of Indian Institute of Technology Madras. The authors are grateful to Dr. A. Venkata Ravindra and Dr. Bhaskar Chandra Behera for their assistance.

[1]A.-M. H. Gosnet and J.-P. Renard, J. Phys. D: Appl. Phys. **36**, R127–R150 (2003).
[2]C. Cui and T. A. Tyson, Appl. Phys. Lett. **84**, 942 (2004).
[3]W. Prellier, P. Lecoeur, and B. Mercey, J. Phys.: Condens. Matter **13**(48), R915 (2001).
[4]A. V. Ravindra, P. Padhan, and W. Prellier, Appl. Phys. Lett. **101**, 161902 (2012).
[5]A. Sahoo, P. Padhan, and W. Prellier, ACS Appl. Mater. Interfaces **9**, 36423–36430 (2017).
[6]S. D. Ha and S. Ramanathan, J. Appl. Phys. **110**, 071101 (2011).
[7]W. Kern, *Thin Film Processses II* (Academic Press, Inc., San Diego, CA, 2012).
[8]Q. Bao, C. Chen, D. Wang, Q. Ji, and T. Lei, Appl. Surf. Sci. **252**, 1538–1544 (2005).
[9]A. B. Posadas, M. Lippmaa, F. J. Walker, M. Dawber, C. H. Ahn, and J. M. Triscone, *Physics of Ferroelectrics* (Springer-Verlag Berlin Heidelberg, 2007), pp. 219–304.
[10]X. X. Xi, G. Linker, O. Meyer, E. Nold, B. Obst, F. Ratzel, R. Smithey, B. Strehlau, F. Weschenfelder, and J. Geerk, Z. Phys. B: Condens. Matter **74**, 13 (1989).
[11]H. C. Li, G. Linker, F. Ratzel, R. Smithey, and J. Geerk, Appl. Phys. Lett. **52**, 1098 (1988).
[12]M. Y. Ali, W. Hung, and F. Yongqi, Int. J. Precis. Eng. Manuf. **11**, 157 (2010).
[13]F. Liu, Y. Li, K. Zhang, B. Wang, C. Yan, Y. Lai, Z. Zhang, J. Li, and Y. Liu, Sol. Energy Mater. Sol. Cells **94**, 2431–2434 (2010).
[14]M. Eshraghi, H. Salamati, and P. Kameli, J. Alloys Compd. **437**, 22–26 (2007).
[15]R. Nori, S. N. Kale, U. Ganguly, N. R. C. Raju, D. S. Sutar, R. Pinto, and V. R. Rao, J. Appl. Phys. **115**, 033518 (2014).
[16]P. Padhan, W. Prellier, and R. C. Budhani, Appl. Phys. Lett. **88**, 192509 (2006).
[17]J.-H. Kim, S. I. Khartsev, and A. M. Grishin, Appl. Phys. Lett. **82**, 4295 (2003).
[18]C. Adamo, L. Méchin, T. Heeg, M. Katz, S. Mercone, B. Guillet, S. Wu, J.-M. Routoure, J. Schubert, W. Zander, R. Misra, P. Schiffer, X. Q. Pan, and D. G. Schlom, APL Mater. **3**, 062504 (2015).
[19]A. K. Pradhan, S. Mohanty, K. Zhang, J. B. Dadson, E. M. Jackson, D. Hunter, R. R. Rakhimov, and G. B. Loutts, Appl. Phys. Lett. **86**, 012503 (2005).
[20]N. Setter, D. Damjanovic, L. Eng, G. Fox, S. Gevorgian, S. Hong, A. Kingon, H. Kohlstedt, N. Y. Park, G. B. Stephenson, I. Stolitchnov, A. K. Taganstev, D. V. Taylor, T. Yamada, and S. Streiffer, J. Appl. Phys. **100**, 051606 (2006).
[21]M. Huijben, L. W. Martin, Y. H. Chu, M. B. Holcomb, P. Yu, G. Rijnders, D. H. A. Blank, and R. Ramesh, Phys. Rev. B **78**, 094413 (2008).
[22]R. P. Borges, W. Guichard, J. G. Lunney, J. M. D. Coey, and F. Ott, J. Appl. Phys. **89**(7), 3868 (2001).
[23]Z. Konstantinovic, J. Santiso, D. Colson, A. Forget, Ll. Balcells, and B. Martínez, J. Appl. Phys. **105**, 063919 (2009).
[24]M. Ziese, I. Vrejoiu, A. Setzer, A. Lotnyk, and D. Hesse, New J. Phys. **10**, 063024 (2008).
[25]A. K. Pradhan, D. Hunter, T. Williams, B. Lasley-Hunter, R. Bah, H. Mustafa, R. Rakhimov, J. Zhang, D. J. Sellmyer, E. E. Carpenter, D. R. Sahu, and J.-L. Huang, J. Appl. Phys. **103**, 023914 (2008).
[26]A. Urushibara, Y. Moritomo, T. Arima, A. Asamitsu, G. Kido, and Y. Tokura, Phys. Rev. B **51**, 14103 (1995).
[27]A. Monsen, J. E. Boschker, F. Macia, J. W. Wells, P. Nordblad, A. D. Kent, R. Mathieu, T. Tybell, and E. Wahlstrom, J. Magn. Magn. Mater. **369**, 197–204 (2014).
[28]A. J. Millis, T. Darling, and A. Migliori, J. Appl. Phys. **83**, 1588 (1998).
[29]P. M. Leufke, A. K. Mishra, A. Beck, D. Wang, C. Kubel, R. Kruk, and H. Hahn, Thin Solid Films **520**, 5521–5527 (2012).
[30]M. Ohring, *The Materials Science of Thin Films* (Academic Press, Inc., San Diego, CA, 1992), p. 105.